Microfluidics

DOI: 10.1002/ange.200500558

# Quantitative Spatial Mapping of Mixing in Microfluidic Systems**

*Steven W. Magennis, Emmelyn M. Graham, and Anita C. Jones**

Microfluidics promises to revolutionize chemical analysis,[1,2] synthesis,[3–5] and biotechnology[6] by combining processes such as mixing, separation, reaction, and detection in a single device. These systems function as "labs-on-a-chip",[7] creating a technology that is low-cost, high-throughput, miniaturized, and automated. Their decreased size imparts microfluidics with many benefits, but miniaturization results in a fundamental change in flow characteristics. Turbulent flow predominates at the macroscale, whereas fluids flow in a laminar fashion at the microscale, without the random mixing that is characteristic of turbulence.[8] These laminar flow conditions mean that multiple fluid streams tend to flow in parallel through microchannels, mixing only by diffusion across their interfaces.[9] Whereas laminar flow behavior has been exploited to good effect in microanalytical systems, many emerging applications of microfluidic devices require rapid and efficient mixing.

Miniaturizing the mixing process has been identified as a major hurdle in the performance and development of microfluidic devices.[10] In labs-on-a-chip, the purpose of mixing is generally to bring together solute species from two (or more) flows. In the laminar flow regime, mixing occurs slowly by diffusion of solute (and solvent) molecules across the flow boundary. For rapid mixing, laminar flow must be disrupted to give chaotic mixing, in which there is bulk transfer of fluid (solvent carrying solute) between the flows.

Micromixers can be either passive (static) or active devices. Passive micromixing strategies frequently rely on diffusion-controlled mixing, with multilamination or flow-splitting techniques to minimize the mixing equilibration time.[11] To increase the mixing rate beyond that limited by diffusion, passive mixers that induce lateral transport of fluid between streams have been devised.[12,13] Active micromixers use miniature stirrers or external fields to chaotically

[*] Dr. S. W. Magennis, E. M. Graham, Dr. A. C. Jones
Collaborative Optical Spectroscopy, Micromanipulation and Imaging Centre (COSMIC)
and the School of Chemistry
The University of Edinburgh
King's Buildings, Edinburgh EH9 3JZ (UK)
Fax: (+44) 131-650-4743
E-mail: a.c.jones@ed.ac.uk

[**] This work was supported by the EPSRC Insight Faraday Partnership, SHEFC and Lab 901 Ltd. We thank Andy Garrie for fabricating the flow cell, and Dave Towers and Ken Macnamara for helpful discussions.

Supporting information for this article is available on the WWW under http://www.angewandte.org or from the author.

intersperse fluid flows. In spite of the increasing attention paid to the mixing problem, devices are still designed by trial-and-error methods.[14] It is therefore essential that techniques that permit the visualization of fluid composition with high quantitative and spatial resolution are found. This will allow testing of prototype devices and will provide essential experimental data to guide the development of theoretical models and to validate computational simulations. Computational fluid dynamics models have proven useful in preliminary mixer designs, but a rigorous understanding of the fundamental principles of microfluidics would lead to the development of better models for complex mixing devices.[15]

The most common methods for visualizing flow and mixing efficiency are fluorescence intensity imaging[9,10,13,16] and transmitted light microscopy with colored dyes, pH indicators, and colored reaction products.[8,15,17] These techniques are relatively cheap, easy to set up, and, in the case of fluorescence imaging, provide excellent contrast. Unfortunately, the ability of these intensity-based techniques to provide a quantitative picture of fluid composition in microfluidic systems is severely limited by their sensitivity to variations in the optical path, instability of the light source, scattering, uncertainty in the dye concentration, and photobleaching effects.[18]

Herein, we describe a superior approach to the imaging of microfluidic systems by using fluorescence lifetime imaging microscopy (FLIM). This technique involves spatially resolving the fluorescence lifetime of a fluorescent dye, rather than the intensity. It overcomes all of the aforementioned problems of intensity-based methods, because the lifetime is independent of the number of fluorescing molecules. To date, the use of FLIM has been restricted to the imaging of biological systems.[19–21] Herein, we demonstrate that FLIM enables spatially resolved quantitation of fluid mixing in microfluidic devices.

Solutions of the fluorescent dye 1,8-anilinonaphthalene sulfonate (ANS) in pure methanol and a water/methanol mixture (1:1 molar ratio, which corresponds to water at 30.8% *v*/*v*) were pumped into a microchannel flow cell to meet head-on at a T-junction, as illustrated in Figure 1a. The flow channels had a depth of 200 μm and a width of 400 μm. The flow rates were varied from 10–75 $\mu L\,min^{-1}$. These dimensions and flow rates correspond to Reynolds numbers of less than 10 so that the fluids are in the laminar flow regime.[17]

Fluorescence lifetime images were obtained by using wide-field illumination of the microfluidic cell with an ultrafast pulsed laser. A gated intensified CCD camera was used to collect the resultant fluorescence within a short time window after a defined delay following the laser pulse. A series of images was acquired by varying the delay time between the detection window and the laser pulse, thereby sampling the entire fluorescence decay of the ANS probe (Figure 1b); the data from each pixel was then fitted to a single exponential decay. ANS was chosen as the dye because its fluorescence lifetime is extremely sensitive to the composition of water/methanol mixtures, showing a near-linear variation from 250 ps in pure water to 6 ns in pure methanol.[22] The calibration curve in Figure 1c, which correlates

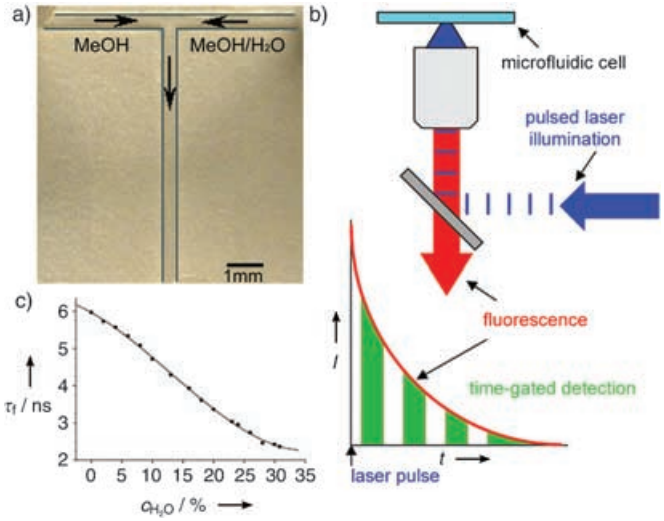


***Figure 1.*** a) Photograph of the microfluidic flow cell, in which arrows indicate the direction of flow; the channel edges have been highlighted for clarity. b) Schematic of fluorescence lifetime imaging microscopy (FLIM). c) Calibration curve showing ANS fluorescence lifetime ($\tau_f$) as a function of the methanol/water ratio in the solution. The following equation gave a good fit to the data: $y = 5.97258 - (0.09267x) - (0.00382x^2) + (9.82168\times10^{-5}x^3)$, in which $y$ is the lifetime in ns and $x$ is the concentration of water (% *v*/*v*) in the water/methanol mixture. The concentration of ANS was 1 mM. Lifetimes were measured by TCSPC. The decays and fitted data are given in the Supporting Information.

the fluorescence decay rate of ANS with the percentage of water in solution, was determined by time-correlated single-photon counting (TCSPC, Supporting Information). ANS displays a single exponential decay at all water/methanol ratios, making it an ideal and unambiguous probe of solvent composition.

The effectiveness of the time-resolved technique is demonstrated in Figure 2, which compares intensity and lifetime images for two regions of the flow cell during a typical experiment. The intensity and FLIM images, which are displayed with the same pseudocolor scale, are noticeably different. The intensity images (Figure 2a) show large, irregular variations in intensity across the field of view, with the regions of highest intensity located near the input of the solution of ANS in methanol. The FLIM images give a clear and unambiguous picture of the liquid composition (Figure 2b). These images show smooth transitions from long to short lifetime (left to right), across a clearly defined mixing region. By using the calibration curve in Figure 1c, the solution composition at each point in the FLIM image can be directly determined. In principle, there should be a clear correlation between the intensity images and the lifetime images; the longer the fluorescence lifetime, the higher the quantum yield and hence the higher the fluorescence intensity (given that the ANS concentration is constant). In practice, however, no such correlation is apparent, and it is clear that the intensity-based images are strongly distorted by variation of the illuminating field, the collection efficiency, and the other variables mentioned above. The microfluidic flow cell

  

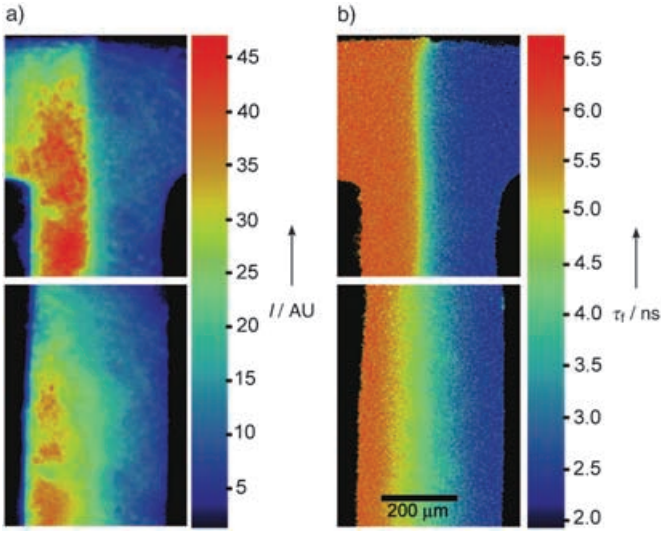


***Figure 2.*** Comparison of a) fluorescence intensity images with b) FLIM images for the mixing of solutions of ANS in pure methanol and ANS in a water/methanol mixture (30:70 *v*/*v*) by using the arrangement shown in Figure 1a. The concentration of ANS in both input solutions was 1 mM, and the flow rate was 50 μL min$^{-1}$. For FLIM, the gate width was 600 ps, and 46 images were recorded at intervals of 500 ps. Every image represents the average of five separate exposures, each with an integration time of 0.1 s and a readout time of 50 ms to give a total acquisition time of about 35 s. The lifetimes of ANS in pure methanol and the equimolar water/methanol solution at the input to the flow cell are the same as those measured by the TCSPC method. The intensity image was constructed by summing the lifetime images, which allows a direct comparison between the time-resolved and intensity-based methods. By using the calibration curve in Figure 1c, the composition of the fluid can be read directly from the FLIM map.

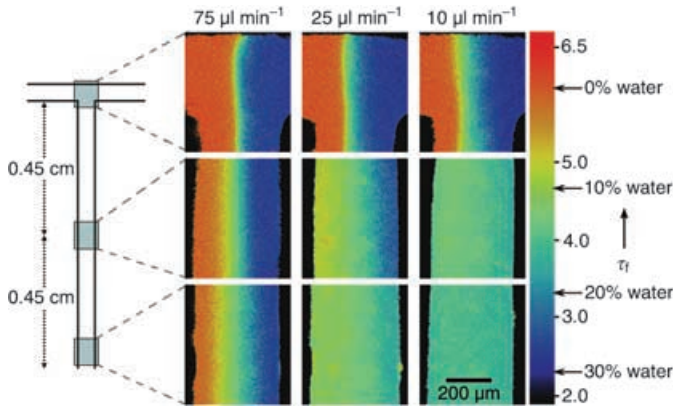


***Figure 3.*** FLIM images for the mixing of solutions of ANS in pure methanol and ANS in a water/methanol mixture (30:70 *v*/*v*), showing the spatial dependence of fluorescence lifetime ($\tau_f$) on the flow rate and the position within the flow cell. Images were acquired at three positions in the flow cell and for three flow rates, as indicated. Other experimental parameters are as described for Figure 2b.

used in this study is of a simple design, and it is likely that intensity-based imaging will be even more prone to optical artifacts in complex devices. FLIM, on the other hand, faithfully reports the fluid composition, as the lifetime is governed solely by the solvent environment of the ANS probe, and is immune to other undesirable effects.

The FLIM technique has been used to monitor mixing as a function of flow rate and flow distance (Figure 3). The compositional variation observed in Figure 3 is indicative of two fluids under laminar flow, as expected. One striking feature of the resultant images is how little mixing occurs in the region where the two input streams meet. Despite being forced together, there is no sign of turbulent mixing. The input streams are well-behaved, with no fluctuations in the position of the boundary between them (Supporting Information). Instead, the two streams stay completely separate, except for a narrow mixing region that results from diffusion. The overall trend is for the mixing region to broaden as the flow rate decreases and as the fluids move further downstream, as expected for diffusion-controlled mixing. For the highest flow rate (75 μL min$^{-1}$), regions that are identical in composition to the input streams persist, even after traveling 1 cm down the channel. In contrast, the two fluids have completely mixed at this distance downstream at the lowest flow rate (10 μL min$^{-1}$).

FLIM allows mixing to be monitored with high spatial resolution (Figure 4a,b); it is possible to accurately measure small changes in the fluid composition in sub-picoliter interrogation volumes. The technique is sensitive enough to reliably detect a change in the volume fraction of approximately 2% (Figure 4c); this is equivalent to a lifetime change of about 250 ps, which is a measurement limit set by the

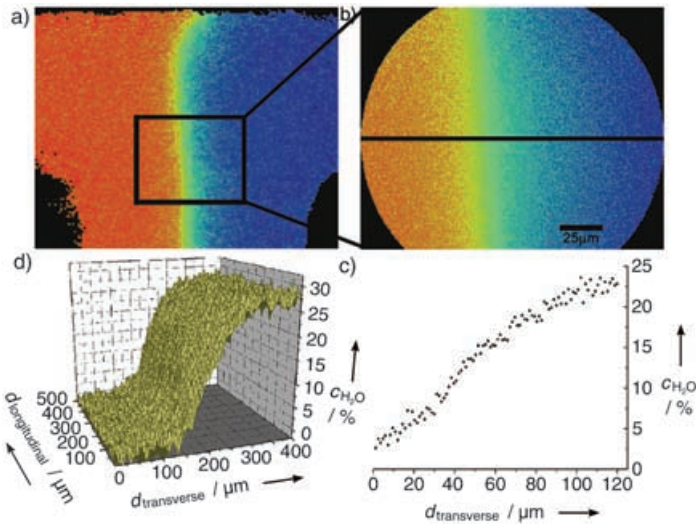


***Figure 4.*** Quantitation of mixing by using FLIM: a) FLIM image of the mixing of methanol and water/methanol with a 20× objective. The arrangement shown in Figure 1a was used, and the flow rate was 75 μL min$^{-1}$. b) Expanded image of the same mixing region from a 100× objective. c) Composition profile along the cross section indicated in Figure 4b. d) Representation of the fluorescence lifetime data in Figure 4a as a composition surface; composition values were calculated with the calibration curve in Figure 1c.

temporal width of the detection windows. The compositional resolution could be improved by increasing the time-resolution of fluorescence detection, using photon counting methods. This method is equally applicable to diffusion-controlled mixing (the fluorescence lifetime responds to the net diffusion of water molecules across the flow boundary) and mixing by mass transport of fluid. Therefore, it is generally applicable to the evaluation of all types of micromixers. The quantitative spatial profiles of fluid composition that can be generated by FLIM (Figure 4c,d) will be particularly valuable for supporting and guiding theoretical models of fluid flow in microfluidic systems.

The present results demonstrate that wide-field FLIM can directly measure the 2D mixing of fluids in microfluidic systems with a level of quantitation that is not available from other methods. It has been shown that intensity-based techniques such as confocal microscopy[13] and optical coherence tomography[23] can provide 3D imaging of microfluidic flows. This is important for cases in which the variations in fluid composition are aligned with the optical axis, as these cannot be resolved by intensity-based wide-field methods.[23] Our wide-field FLIM technique would, however, detect nonuniform mixing along the optical axis, that is, the depth axis of the microchannel, as the superposition of a number of layers of varying composition along this axis would result in the observation of a multiexponential fluorescence decay, rather than the single exponential decay characteristic of uniform mixing throughout the depth of field. The FLIM approach can be extended to full 3D imaging with confocal or multiphoton excitation without loss of the attendant benefits of time-resolved detection that have been established herein. In this version of the technique, the tightly focused excitation laser beam is raster-scanned across the sample, and the fluorescence decay is acquired point-by-point, using TCSPC. The use of multiphoton excitation would also enhance imaging penetration through strongly absorbing or scattering fluids and structures.

The mixed solvent system reported herein, in conjunction with the ANS probe, was devised purely as a measurement tool for the generic study of micromixing, and was not intended to relate to any specific applications of lab-on-a-chip systems. Our approach is, however, generally applicable to any solvent system, as long as there is a change in molecular environment upon mixing that results in variation in the fluorescence lifetime of an appropriate probe. For example, the mixing of aqueous solutions could be studied by using streams of different pH that incorporate a pH-sensitive dye, such as a seminaphthorhodafluor (SNARF) probe. Alternatively, streams containing different concentrations of a collisional quencher, such as iodide, could be used. In view of the flexibility of this approach, we anticipate that FLIM will become an essential tool in the design, modeling, and evaluation of microfluidic systems.

## Experimental Section

All measurements were made with the ammonium salt of ANS (Fluka, used as received). The methanol and water used in this study were HPLC grade (Fisher Scientific) and were used as received. Solutions of ANS ($\approx 1$ mM) were stored in the dark, and the lifetime of ANS fluorescence at room temperature was used as a routine check of sample purity after storage. No emission could be detected from the solvents under the instrumental conditions employed. Time-resolved fluorescence spectroscopy was performed by using the technique of TCSPC as described previously.[22]

The microfluidic cell was fabricated from Perspex with the T-shaped channel milled out to a depth of 0.2 mm using an end mill of diameter 0.4 mm (Drill Service Ltd.). The three inlet/outlet holes were drilled 1.6 mm in diameter and fitted with polypropylene tubing. The cell was sealed by gluing (Norland Optical Adhesive No. 61) a cover-glass over the channels, and was attached to syringes with silicone tubing. The flow of fluids from the syringes was controlled by a syringe pump (Univentor 802, Univentor Ltd.).

For FLIM, frequency-doubled light from a mode-locked Ti sapphire laser ($\lambda = 400$ nm, repetition rate = 4.75 MHz) was expanded, collimated, and directed into a Nikon TE300 inverted microscope operating in an epifluorescence configuration. This excitation light was reflected from a dichroic filter (DM430, Nikon) and focused onto the microfluidic flow cell with either 20× (PA, NA = 0.75, Nikon) or 100× (Ph3, NA = 1.3, oil immersion, Nikon) objectives. The laser power incident on the flow cell was typically $\approx 100$ μW. The resultant fluorescence was collected through the same objective, passed through a barrier filter (515–555 nm, Nikon) and imaged onto a Picostar HR-12QE gated intensified CCD camera system (LaVision GMBH, Berlin). The excitation beam was split, and one portion was used to trigger a fast photodiode. The photodiode output was passed through a constant fraction discriminator (CF4000, Ortec), and used as the trigger signal for the Picostar system. The experiments described herein were recorded with a gate width of 600 ps, which was measured by detecting laser light reflected from a mirror (the minimum gate width for this camera is 200 ps). The intensifier gate was delayed relative to the laser trigger signal by using a DEL150 picosecond delay module (Becker and Hickl). The 12-bit CCD camera is a progressive scan interline sensor (1370(H) × 1040(V) pixels; pixel size = 6.45 × 6.45 μm$^2$). Images were the average of five separate exposures, were recorded in steps of 500 ps over a range of 23 ns, and employed 4 × 4 hardware binning. The integration time for each image was 100 ms, with a readout time of 50 ms to give a total acquisition time of approximately 35 s. The excitation intensity was adjusted to give a peak intensity of 3000–4000 counts in the brightest image, which corresponds to the start of the fluorescence decay. The background signal of $\approx 50$ counts was subtracted from each image. DaVis 6.2 software running the Picostar DaVis module was used to control the Picostar system and delay card, and to analyze the data. The peak of the fluorescence intensity was found in the fourth image of the image series. To ensure that the instrument response did not interfere with the fitting, the first five images were not used for analysis. The sixth image (which was 1 ns after the peak) and subsequent images were analyzed to allow a decay curve to be constructed for each pixel. Pixels with low counts in the first analyzed image (typically 700 counts) were removed at this stage. Each of these curves was then fitted to a single exponential decay. A lifetime map was produced by assigning a color on a 16-bit pseudocolor scale to each of the fitted lifetimes, and these were displayed over a range of 2.0–6.8 ns.

Received: February 15, 2005
Revised: June 24, 2005
Published online: September 21, 2005

**Keywords:** fluorescence · imaging · microfluidics · microreactors · mixing

  

[1] T. Vilkner, D. Janasek, A. Manz, *Anal. Chem.* **2004**, *76*, 3373.
[2] A. Hibara, M. Nonaka, M. Tokeshi, T. Kitamori, *J. Am. Chem. Soc.* **2003**, *125*, 14954.
[3] S. Xu, Z. Nie, M. Seo, P. Lewis, E. Kumacheva, H. A. Stone, P. Garstecki, D. B. Weibel, I. Gitlin, G. M. Whitesides, *Angew. Chem.* **2005**, *117*, 734; *Angew. Chem. Int. Ed.* **2005**, *44*, 724.
[4] H. Song, J. D. Tice, R. F. Ismagilov, *Angew. Chem.* **2003**, *115*, 792; *Angew. Chem. Int. Ed.* **2003**, *42*, 768.
[5] P. D. I. Fletcher, S. J. Haswell, E. Pombo-Villar, B. H. Warrington, P. Watts, S. Y. F. Wong, X. Zhang, *Tetrahedron* **2002**, *58*, 4735.
[6] M. U. Kopp, A. J. de Mello, A. Manz, *Science* **1998**, *280*, 1046.
[7] D. R. Reyes, D. Iossifidis, P.-A. Auroux, A. Manz, *Anal. Chem.* **2002**, *74*, 2623.
[8] B. Zhao, J. S. Moore, D. J. Beebe, *Science* **2001**, *291*, 1023.
[9] B. H. Weigl, P. Yager, *Science* **1999**, *283*, 346.
[10] H. Chen, J.-C. Meiners, *Appl. Phys. Lett.* **2004**, *84*, 2193.
[11] L. E. Locascio, *Anal. Bioanal. Chem.* **2004**, *379*, 325.
[12] T. J. Johnson, D. Ross, L. E. Locascio, *Anal. Chem.* **2002**, *74*, 45.
[13] A. D. Stroock, S. K. W. Dertinger, A. Ajdari, I. Meziæ, H. A. Stone, G. M. Whitesides, *Science* **2002**, *295*, 647.
[14] J. M. Ottino, S. Wiggins, *Science* **2004**, *305*, 485.
[15] F. Schönfeld, V. Hessel, C. Hofmann, *Lab Chip* **2004**, *4*, 65.
[16] M. S. Munson, P. Yager, *Anal. Chim. Acta* **2004**, *507*, 63.
[17] P. J. A. Kenis, R. F. Ismagilov, G. M. Whitesides, *Science* **1999**, *285*, 83.
[18] R. M. Clegg, O. Holub, C. Gohlke, *Methods Enzymol.* **2003**, *360*, 509.
[19] F. G. Haj, P. J. Verveer, A. Squire, B. G. Neel, P. I. H. Bastiaens, *Science* **2002**, *295*, 1708.
[20] T. W. J. Gadella Jr., T. M. Jovin, *J. Cell Biol.* **1995**, *129*, 1543.
[21] J. R. Lakowicz, H. Szmacinski, K. Nowaczyk, M. L. Johnson, *Proc. Natl. Acad. Sci. USA* **1992**, *89*, 1271.
[22] L. Dougan, J. Crain, H. Vass, S. W. Magennis, *J. Fluoresc.* **2004**, *14*, 91.
[23] C. Xi, D. L. Marks, D. S. Parikh, L. Raskin, S. A. Boppart, *Proc. Natl. Acad. Sci. USA* **2004**, *101*, 7516.

  